Free-energy model for fluid atomic helium at high density

Josep M. Aparicio

Centre d'Estudis Avançats de Blanes, Consejo Superior de Investigaciones Científicas, 17300 Blanes, Spain

Gilles Chabrier

Laboratoire de Physique (CNRS), Ecole Normale Supérieure de Lyon, 69364 Lyon Cedex 07, France

We develop a free-energy model aimed at describing the thermodynamics of fluid atomic helium at high density and high temperature. This model represents a step towards a consistent description of the pressure ionization of helium, as encountered in astrophysical situations and high-pressure experiments. In the present paper, a perturbation theory is developed to derive the configuration energy of helium at high density, and the modification of internal states in the partition function due to N-body effects is treated self-consistently within an occupation probability formalism. A scaling relationship between the internal levels and the ground state of helium is presented, which reproduces the experimental energy spectrum of helium within 3%. We also develop a *density-dependent* pair potential for helium, which reduces to the *ab initio* Ceperley-Partridge potential [D. M. Ceperley and H. Partridge, J. Chem. Phys. **84**, 820 (1986)] at low density and includes implicitly the many-body effects at high density. The theoretical Hugoniot curves and the speed of sound derived from our free-energy model are in excellent agreement with the available experimental data, thereby assessing the validity of the present model at high density. These calculations are the extension of a former model for hydrogen [D. Saumon and G. Chabrier, Phys. Rev. A **44**, 5122 (1991)] to nonhydrogenic, two-electron systems. The present free-energy model can be used to derive an accurate equation of state for the outermost layers of Jovian planets, brown dwarfs, and white dwarfs.

PACS number(s): 52.25.−b, 05.30.−d, 05.70.Ce

I. INTRODUCTION

The understanding of the physical properties of matter under extreme thermodynamic conditions is a crucial problem in dense matter physics, as much from a fundamental viewpoint as for physical and astrophysical applications. The equations of state (EOS) of dense hydrogen and helium are of particular interest as much for the interpretation of high-pressure experiments [1], and the impending pressure ionization problem, as for the derivation of reliable interior models for dense astrophysical objects. The interior of Jovian planets and brown dwarfs [2], and the external layers of white dwarfs [3], are made up essentially of helium and hydrogen. Under the thermodynamic conditions encountered in these objects, the helium and hydrogen atoms experience temperature and *pressure* ionization. This partial ionization region is the source of pulsation instabilities in stars and Jovian planets so that a correct description of this domain is crucial for a correct understanding of the internal structure, the evolution, and the seismological properties of dense stellar and planetary objects [4].

A complete free-energy model for fluid hydrogen at high density has been proposed recently which leads to a consistent description of pressure molecular dissociation and ionization [5,6]. The present model is essentially an extension of the previous hydrogen model to helium. The case of He-like systems is more complicated because of the nonhydrogenic behavior of the system, and special care must be taken when calculating the contribution arising from the internal levels.

The present paper is devoted to the derivation of a free-energy model for *neutral* helium only. Ionization, and the problem of *pressure* ionization, will be considered in a future companion paper.

The paper is organized as follows: In Sec. II we present the general free-energy model for the atomic helium fluid. The configuration free energy, calculated from an effective interatomic potential, is described in Sec. III. In Sec. IV, we present the treatment of the internal levels, and the scaling law between the ground state and the excited levels in the internal partition function (IPF), which enable us to connect hydrogenic and nonhydrogenic systems. An extension of previous work beyond the so-called low-density and low-excitation approximations for the interaction between atoms in different quantum states is also presented in this section. The general model is summarized at the end of Sec. IV. Comparison with experiments and analysis of the results are discussed in Sec. V, whereas Sec. VI is devoted to examination of the different contributions to the total free energy and pressure. The conclusion is presented in Sec. VII.

II. THE FREE-ENERGY MODEL

The present paper is limited to a description of atomic, i.e., nonionized, helium, and is therefore restricted to low temperature ($\log_{10} T \lesssim 4.2$) and low density ($\log_{10} \rho \lesssim 1$).

The first limit corresponds to the onset of ionization, as estimated from the Saha equations, whereas the second limit corresponds to the density where the Fermi energy

of the electrons equals their binding energy on the nucleus. Our model relies on the so-called chemical picture, assuming that bound configurations, atoms or molecules, retain a definite identity, and interact through pairwise additive potentials. This approach has been discussed extensively elsewhere (see [6] and references therein). Because all particles are very nearly classical in the regime of interest, we can factorize the partition function and treat the small quantum effects within a semiclassical approximation. If we make the additional assumption that the internal levels of atoms are only weakly affected by the presence of nearby particles (the limits of such an assumption will be discussed in detail in the text), the partition function can be factorized out into translational, configurational, internal, and quantum contributions, so that the Helmholtz free energy reads

$$F = F_{id} + F_{int} + F_{conf} + F_{qm} . \tag{1}$$

The first term on the right-hand side (rhs) of Eq. (1), that is, the ideal gas free energy, represents the purely translational degrees of freedom of the atoms, which obey the Maxwell-Boltzman distribution. The last three contributions are discussed separately in the following sections. He_2 is not a stable configuration at the temperatures considered in the present calculations and is not included in the model.

III. THE CONFIGURATIONAL FREE ENERGY

A. The He-He pair potential

Interaction potentials are central to the concept of configuration energy. We have evaluated the configuration term in the context of pairwise additive potentials, which tremendously simplifies the calculations. At high density, this approximation becomes incorrect and we must consider density-dependent potentials, which require a solution of the general quantum N-body problem. Fortunately, this problem can be partially circumvented by using experimentally determined effective pair potentials which include many-body effects implicitly. Such a pair potential has been derived by Nellis et al. [1] from shock-compression experimental data up to temperatures $T \sim 20\,000$ K and pressures $P \sim 0.6$ Mbar. It takes the simple form

$$\phi(r) = Ae^{-br} ,$$

with $A = 1.1 \times 10^5 \epsilon k_B$ and $b = 11.0/r_m$, $\epsilon = 10.8$ K and $r_m = 2.9673$ Å being, respectively, the depth and the radius of the minimum of the Aziz potential [7]. By construction, the many-body effects present at the highest pressures reached are implicitly included in this effective pair potential.

The aforementioned potential, however, was obtained with a different model free energy [1]. We have derived a new potential, aimed at reproducing not only the same high-density experimental data, but also low-density results within *our* model. At very low densities an *ab initio* *two*-body potential is accurate enough to describe the interactions between particles. As mentioned above, such a scheme fails at higher densities because of the importance

of N-body effects, which soften the repulsive part of the potential [8,9]. We have derived a *density-dependent* potential which reproduces high-density experimental results and which at low density reduces to the accurate two-body Ceperley-Partridge [10] potential V_{CP}, obtained from quantum Monte Carlo calculations. Our model potential reads

$$\phi(r) = \left[(1-C) + \frac{C}{1+D\rho} \right] V_{CP}(r) . \tag{2}$$

The parameters C and D mimic the softening effect of the many-body interactions in the pair potential, whose qualitative behavior remains unchanged. Reproduction of the experimental Hugoniots [1] yields the optimized values $C = 0.3564$ and $D = 7.735$ cm^3/g, to be used throughout the present calculations. Figure 1 shows potential (2) in its zero-density limit and at high density, and compares it with the potential derived by Nellis et al. [1].

As will be shown in Sec. V A, potential (2) accurately reproduces shock-wave and speed of sound experimental results over the whole density range presently available. The effect of the stiffness of the potential on the results will also be examined carefully in Sec. V A.

B. Perturbation theory

To compute the configuration energy associated with the pair potential, we rely on the so-called Weeks-Chandler-Andersen [11] (WCA) perturbation theory. This theory was derived initially for the liquid state, but was later on extended at high density and high tempera-
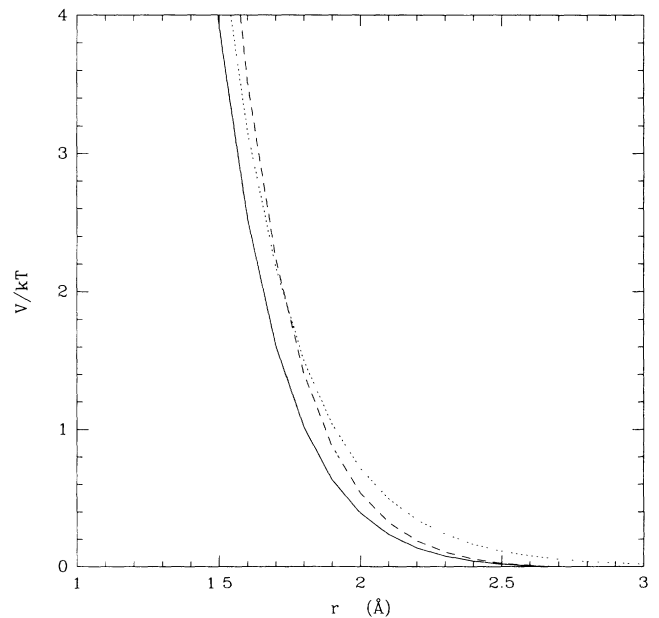

FIG. 1. Comparison between the potential (2) at zero density (dashed line) and at $\log_{10}\rho = 1$ (solid line), and the potential of Nellis et al. [3] (dotted line). The temperature used to normalize the potential is 1000 K.

ture for one-component systems [12] and binary mixtures [13]. Within the framework of the WCA theory, the interparticle potential is split into a reference and a perturbation part:

$$\phi(r) = \phi_{ref}(r) + \phi_{pert}(r) .$$

Truncating the free-energy expansion after the first order, the so-called high-temperature approximation [11] (HTA), the configurational free energy reads

$$F_{conf}(N, V, T)$$
$$= F_{ref}(N, V, T) + \frac{N^2}{2V} \int \phi_{pert}(r) g_{ref}(r) d^3r . \quad (3)$$

The separation of the potential into the reference part and the perturbation part was computed by using a modification of the procedure of Kang et al. [12], namely,

$$\phi_{pert}(r) = \begin{cases} \phi(\lambda) + \left[\dfrac{d\phi}{dr}\right]_{r=\lambda}(r-\lambda), & r < \lambda \\ \phi(r), & r > \lambda \end{cases} \quad (4)$$

where $\lambda = (a_{fcc}^{-3} + r^{*-3})^{-1/3}$ denotes the density-dependent breakpoint [note the modification from the definition used in the standard procedure of Kang et al., $\lambda = \min(a_{fcc}, r^*)$, in order to obtain a continuously differentiable λ], where $a_{fcc} = (\sqrt{2}/n)^{1/3}$ is the fcc interparticle distance (n is the particle number density) and r^* is the location of the minimum of the potential.

The reference system is approximated by a hard-sphere fluid, for which analytical expressions exist for the free energy [14] and the pair correlation function [15,16]. The pair correlation function entering Eq. (3) is given by

$$g_{ref}(r) \approx \exp[-\beta V_{ref}(r)] y_{HS}(r) ,$$

and not by $g_{HS}(r)$ [17]. This is of prior importance when evaluating the quantum correction, as will be seen in Sec. V E. The hard-sphere diameter σ is calculated through the WCA criterion [18], by equating the compressibilities of the true reference system and the hard-sphere fluid:

$$\int_0^\sigma y^{HS}(r) \exp[-\beta\phi_{ref}(r)] d^3r$$
$$+ \int_\sigma^\lambda g^{HS}(r)\{\exp[-\beta\phi_{ref}(r)] - 1\} d^3r = 0 . \quad (5)$$

Since Eq. (5) has to be solved for each given temperature and density, the hard-sphere diameter is *temperature and density dependent*, which leads to an implicit dependence of the configuration energy on these two variables, a necessary condition to derive a reliable free-energy model.

IV. THE INTERNAL FREE ENERGY

A. The occupation probability formalism

The internal contribution of N *noninteracting* atoms to the free energy reads

$$F_{int}^0(N, T) = -NkT \ln Z = -NkT \ln \sum_i g_i e^{-\beta\epsilon_i} , \quad (6)$$

where i runs over all bound states, and g_i and ϵ_i denote, respectively, the multiplicity and the energy of state i. As is very well known, Eq. (6) diverges for isolated atoms, due to the infinite number of states clustering near the continuum level. This unphysical behavior is circumvented by the presence of the surrounding interacting particles which remove the highly excited states into the continuum, providing a physical cutoff of the internal partition function. This effect of the surrounding particles on the internal states of the atom is a key problem in describing pressure ionization. The treatment of this problem is included in the present model within the so-called occupation probability formalism (OPF) [19]. This formalism offers numerous advantages over other procedures when treating pressure ionization, but most of all it ensures statistical-mechanical consistency between the description of the interactions of the particles in their ground state, i.e., the configuration energy, and the effect of these interactions on the internal partition function, i.e., the internal free energy. Moreover, it ensures the continuity of the free energy and its derivatives when states are removed from the internal partition function into the continuum, avoiding the discontinuities inherent to other phenomenological descriptions of N-body effects. A complete description of this formalism has been presented extensively in previous work [19,5], and will be only briefly summarized in the context of the present problem. Within the OPF, the internal free energy is rewritten [19]:

$$F_{int} = -NkT \ln\tilde{Z} + f - \sum_i N_i \frac{\partial f}{\partial N_i} , \quad (7)$$

where $f \equiv f(V, T, \{N_i\})$ denotes the nonideal part of the free energy, which depends explicitly on the population of each bound state, N_i, with $\sum_i N_i = N$, and $\tilde{Z}$ defines the modified partition function of the *interacting* system:

$$\tilde{Z} = \sum_i \omega_i g_i e^{-\beta_i \epsilon_i} . \quad (8)$$

In Eq. (8), ω_i is the occupation probability of state i in the interacting system, defined by

$$\omega_i = e^{-\beta(\partial f/\partial N_i)} , \quad (9)$$

so that the population of the state i in the interacting fluid is given by

$$\frac{N_i}{N} = \frac{\omega_i g_i e^{-\beta\epsilon_i}}{\tilde{Z}} = \frac{g_i e^{-\beta(\epsilon_i + \partial f/\partial N_i)}}{\tilde{Z}} . \quad (10)$$

Again, it is important to stress that the occupation probability, which describes the probability that a bound state can actually exist in the midst of the perturbations of the surrounding particles, is computed *self-consistently* with the nonideal term through Eq. (9). This ensures consistency between the *external* interaction, related to the interparticle potential, and its *internal* effect on bound states.

The computation of the OPF requires knowledge of the excitation energies of the unperturbed atom ϵ_i, and a model interaction free energy f for the excited states.

The former are obtained from spectroscopy measurements [20]. The choice of f will be discussed in Sec. IV D.

B. The scaling law for the internal states of helium

An exact solution of the problem of interest would require knowledge of the interaction potentials between *each* internal state. Of course, such information does not exist, and only interaction potentials between atoms in their *ground state* are available. Given this lack of information, we rely on the usual approximation of the interaction between excited states by a hard-sphere model [19]. The hard sphere associated with each quantum state mimics the spatial extension of the electronic orbitals of this state, which leads to a reduction of the phase space available to the other particles. A consistent description of this effect requires a scaling law between the hard-sphere diameter σ_1 for the ground state, determined by Eq. (5), and the diameter σ_i of each state i. Whereas such a scaling law can easily be derived analytically from quantum mechanics for hydrogenic systems [21,5], it is more complicated for helium because (i) the helium wave functions are not known analytically and (ii) the possibility exists for the two electrons to be in two different levels, i.e., on two different orbitals. Moreover, the accurate numerical calculation of the eigenfunctions is extremely cumbersome. Since we only need the mean radius associated with the wave function, we will rather use a simpler, analytical approach, which is accurate enough for our purpose.

The presence of doubly excited states requires special attention. The problem is simplified by the fact that, for the isolated atom, these states lie above the first continuum level, i.e., they are self-ionizing states. However, only *true* bound states, i.e., bound states with an infinite (or at least long enough) lifetime, can be treated within the OPF [19]. A complete treatment of self-ionizing states within the OPF formalism would require time-dependent occupation probabilities, taking into account the lifetime of the state. Therefore, the only excited states to be considered in the present treatment are the singly excited states. However, as seen from Eqs. (9) and (17) below, a singly excited state may eventually occupy a larger volume, and then have a smaller occupation probability, than a doubly excited states, above a certain density. This particular effect will be examined carefully in Sec. V D, where we compare the results when self-ionizing states are included in the IPF.

The treatment of the singly excited states can be first outlined by the following schematic approach: For singly excited states, the inner electron lies close to the nucleus and then feels a nearly unscreened charge $Z_{eff}=2$, whereas for the outer, excited electron, the interaction with the nucleus is screened by the inner electron, so that it feels an effective screened charge $Z_{eff}\sim 1$. The equivalent Bohr radius (maximum of probability) for the excited electron is then at least $r \approx n^2 a_0 = 4a_0$, where a_0 is the hydrogen Bohr radius, whereas it is $r_0 \approx \frac{1}{2}a_0$ for the inner electron ($1s2s$ configuration). There is about a factor 8 between the average positions of the two electrons.

This justifies the hydrogenic approximation for the treatment of the excited states.

The problem is more complicated for the ground state, since the two electrons are at the same distance from the nucleus. However, it has been shown recently [22] that it is possible to make a semiclassical description of the helium atom, i.e., a quantization of the action over cyclic orbits, as is usually done for hydrogenic systems (Bohr model). Such a quantization usually fails for classically nonperiodic systems like the helium atom (three-body problem). However, a classically chaotic system has in fact marginally periodic orbits, which turn out to be unstable. The crucial point is that the states of the *quantum* system are not arbitrarily spread out in the classical phase space but (i) usually do *not* show chaotic behavior, and (ii) are strongly clustered around *classical, periodic* orbits, similar to the clustering of the $1s$ state around the Bohr radius for hydrogen [23,22]. Therefore, whether the classical system is intrinsically periodic (H-like systems) or periodicity appears marginally (He-like systems), the quantum states *are* the quantized classical periodic states, thus justifying a Bohr model approach. In this scheme, the ground state can be identified in the classical problem as two co-orbital electrons, located on each side of the nucleus. We thus obtain the following interaction potential for each electron:

$$V_{eff}(r) = -\int F(r)dr = -\int \left[\frac{Ze^2}{r^2} - \frac{e^2}{(2r)^2} \right] dr$$
$$= -\frac{Z_{eff}e^2}{r}, \qquad (11)$$

with $Z_{eff} = Z = \frac{1}{4}$, which defines an effective Bohr radius for He:

$$a_{0_{eff}} = \frac{a_0}{Z_{eff}} = \frac{4}{7}a_0 . \qquad (12)$$

This equivalent Bohr radius corresponds to the position of the *maximum* of the $1s^2$ wave function. Nearly the same value $(0.6a_0)$ is obtained from Hartree-Fock calculations [24]. As a comparison, the variational method using an equivalent hydrogenic wave function gives $Z_{eff} = Z - \frac{5}{16}$ [25], i.e., a discrepancy of about 3%. We stress, however, that Eq. (12) can be used also for *doubly excited states,* where no variational result exists, and then will be used in our calculations. Within the OPF, the scaling law is based on the *mean* radius $\langle r \rangle$ [19]. For hydrogen,

$$\frac{\langle r \rangle}{r_{max}} = \frac{\langle r \rangle}{a_0} = 1.5$$

for the ground state. Keeping the same ratio for helium [since the potential (11) is hydrogenic], we get $\langle r \rangle = 1.5 a_{0_{eff}} = \frac{6}{7}a_0$ for the ground state of helium, a fairly reasonable agreement with the exact value $0.929a_0$ [26].

In summary, the internal states of helium can be treated within the framework of the following model: (1) Singly excited states of He are treated within the hydro-

TABLE I. Binding energies for the ground state and some excited states of helium, in eV. The experimental values are from Martin's paper [20].

State	Expt.	Theor.	Model
$1s^2$	79.0059	83.33	Semiclassical
$\langle 1s2s \rangle$	58.9870	57.81	Hydrogenic
$\langle 1s3s \rangle$	56.2367	55.93	Hydrogenic
$\langle 1s4s \rangle$	55.3918	55.26	Hydrogenic
$\langle 1s5s \rangle$	55.0239	54.96	Hydrogenic
$2s^2$	21.14	20.83	Semiclassical

genic approximation, and (2) the ground state and doubly excited states are treated within the semiclassical approach, with an equivalent Bohr radius for the ground state $a_{0_{\text{eff}}} = \frac{4}{7} a_0$, where a_0 is the hydrogen Bohr radius.

For helium atoms, the l levels are no longer degenerate, as for hydrogen, and the radii of the internal states must include an l dependence. Taking this fact into account, the scaling law for the singly excited states of helium reads

$$\langle \bar{r}_1 \rangle = \tfrac{6}{7} a_0 , \tag{13a}$$

$$\langle \bar{r}_i \rangle \equiv \langle \bar{r}_{nl} \rangle = \frac{a_0}{2} [3n^2 - l(l+1)], \quad i > 1 . \tag{13b}$$

Equation (13a) represents the *ab initio* limit for the ground state. Since no value exists at high density, we elected *a priori* to choose the density-dependent WCA diameter (5), which stems from the optimization of the configurational energy. Therefore, renormalization of Eq. (13a) leads to the final scaling law for helium internal levels:

$$\sigma_1 = \sigma_{\text{WCA}}(N/V, T) , \tag{14a}$$

$$\sigma_i \equiv \sigma_{nl} = \tfrac{7}{4} \sigma_1 \left[n^2 - \frac{l(l+1)}{3} \right], \quad i > 1 . \tag{14b}$$

This scaling represents the most reasonable choice for the purpose of our calculations. Moreover, Eq. (14a) ensures self-consistency between the configuration free energy and the internal free energy in our model.

In Table I we compare the binding energies obtained from the semiclassical approximation

$$E_n(\text{He}) = -2[13.6 \text{ eV}/n^2]Z_{\text{eff}}^2 ,$$

with $Z_{\text{eff}} = \tfrac{7}{4}$, for helium ground state and *doubly* equally excited states, and from the hydrogenic approximation for the *singly* excited states [Eq. (14b)], with the experimental results [20]. The largest disagreement, which occurs for the $1s^2$ state, is found to be less than 4%, a fairly reasonable result, given the simplicity of our model. This assesses the validity of the scaling law (14) to calculate the radii of the excited states entering the internal partion function of helium.

C. Beyond the *low-excitation* approximation

In all previous calculations [19,5], the occupation probabilities have been calculated within the so-called low-

excitation approximation (LEA) [19]. This approximation assumes that all perturbers α interacting with a given particle β in a quantum state i reside in their ground state, i.e., $i_\alpha = 1 \; \forall \alpha \neq \beta$. Such an approximation fails as soon as the population of excited states becomes substantial, as may occur as temperature rises. Going beyond such an approximation requires a minimization of the free energy with respect to *all* the individual level populations $(N_i)_\alpha$, a tremendously cumbersome numerical task. However, when the excitation energies of the atom are large enough, i.e., when the number of excited states with a nonzero population remains limited, the problem can be solved by using an iterative procedure, taking as initial solutions the populations obtained within the low-excitation approximation. The process converges quite rapidly. In this case, the free energy f no longer depends linearly on the level populations, so that the term $[f - \sum_i N_i(\partial f/\partial N_i)]$ in Eq. (7) does not cancel out, as in the low-excitation approximation (see [19] for details).

D. Beyond the *low-density* approximation (LDA)

For the sake of simplicity, only the term linear in density, i.e., the excluded volume contribution in the hard-sphere free energy, had been retained to describe the interaction free energy f between excited states in previous work [19,5]. In this case, the free energy f in Eq. (7) reads

$$f = f_{\text{HS}}^{(1)} = \frac{\pi kT}{12V} \sum_{i,j} N_i N_j (\sigma_i + \sigma_j)^3 . \tag{15}$$

The remaining, nonlinear, terms were included only in the configuration energy of the *ground* state (see [5]). Again, this approximation becomes spurious at high density. In the present calculations, the full equation of state of the hard-sphere fluid has been included in the IPF for *all* internal states. Thus the final internal free energy, including the complete calculation of the interaction between excited states, beyond the low-excitation approximation and the low-density approximation, reads

$$F_{\text{int}}(\{NH_i\}, V, T)$$

$$= -NkT \ln \tilde{Z} + \left[f_{\text{HS}}(\{N_i\}, V, T) \right.$$

$$\left. - \sum_i N_i \frac{\partial f_{\text{HS}}(\{N_i\}, V, T)}{\partial N_i} \right] , \tag{16}$$

where $f_{\text{HS}}(\{N_i\})$ is the free energy of a *multicomponent* hard-sphere fluid [14], N_i is the number of particles in a quantum state $i \equiv (n,l)$, with an associated hard-sphere diameter σ_i, $\tilde{Z}$ is the IPF in the interacting fluid given by Eq. (8), and the occupation probability ω_i of the quantum state i is given by

$$\omega_i = \exp\left[-\beta \frac{\partial f_{\text{HS}}(\{N_i\}, V, T)}{\partial N_i} \right] . \tag{17}$$

The interaction term f_{HS} with the occupation probability (17) reduces to Eq. (15) at low density (LDA) and to

$$f = \frac{\pi N k T}{6V} \sum_i N_i (\sigma_i + \sigma_l)^3 \tag{18}$$

at low density *and* low temperature (LDA+LEA). Equation (17) ensures a continuous state by state cutoff in the IPF as the density increases [19].

E. The final free-energy model

The previous calculations lead to the following free-energy model for atomic helium:

$$\frac{\beta F(N,V,T)}{N} = \left[\ln \frac{N}{V} \left[\frac{2\pi\hbar^2}{MkT} \right]^{3/2} - 1 \right] \tag{19a}$$

$$- \ln \sum_i \omega_i g_i e^{-\beta\epsilon_i} + \left[\frac{\beta f_{HS}(\{N_i\},\{\sigma_i\})}{N} - \sum_i N_i \frac{\beta \partial f_{HS}(\{N_i\},\{\sigma_i\})}{\partial N_i} \right] \tag{19b}$$

$$+ \frac{\beta}{2} \frac{N}{V} \int \phi_{pert}(r) e^{-\beta\phi_{ref}(r)} y_{HS}(N/V,\sigma_l,r) d^3r \tag{19c}$$

$$+ \frac{\hbar^2\beta^2}{24M} \frac{N}{V} \int \nabla^2\phi(r) e^{-\beta\phi(r)} y_{HS}(N/V,\sigma_1,r) d^3r \ . \tag{19d}$$

The diameters σ_i of the hard spheres are determined by the WCA criterion (5) for the ground state ($n=1$), and by the scaling law (14b) for the excited states; the occupation probabilities ω_i are given by Eq. (17). The individual populations N_i for each excited state are given by Eq. (10), with $\sum_i N_i = N$, where N is constant since no chemical or ionization reaction occurs. The terms (19a) and (19d) represent, respectively, the translational contribution and the quantum contribution to the total free energy. This latter will be discussed in detail in Sec. V E. A total of ten states, i.e., states with $n \leq 4$ for all l, have been included in the internal partition function, with the exact spectroscopically determined energies [20]. Including more states in the IPF is completely inconsequential on the final results. The zero of energy is the energy of the isolated He^{2+} ion, so that the ground state energy of the He atom is

$$E_{binding} = -79.0059 \text{ eV} \ .$$

The effect of the N-body interactions between the particles in *any* quantum state $i \geq 1$ enters in the terms ω_i and f and in the HTA term in Eqs. (19b) and (19c).

V. RESULTS AND COMPARISON WITH EXPERIMENTS

We have applied the free-energy model (19) in the domain $\log_{10}\rho \lesssim 1$ and $\log_{10}T \lesssim 4.2$ in the fluid phase. At densities and temperatures above these limits, pressure or temperature ionization becomes important, and is outside the scope of the present paper. We examine in this section the influence of the different physical inputs of the model on the final results. A subset of these results is presented in Table II, parts (a)–(c), for three isotherms. For each density point, we give the total pressure, entropy, internal energy, and specific heat. Table III gives the variation of the occupation probability of the ground state, the only significantly populated state within the limits of the present model ($N_{i>1}/N_1 \simeq 0 \ \forall\rho$), as will be shown below, as a function of density for three isotherms.

TABLE II. (a) Equation of state along the $\log_{10}T=3$ isotherm. For each density ρ, the entries are the pressure P, the entropy S, the internal energy U, and the specific heat c_v. Units are in cgs. (b) Same as (a) for $\log_{10}T=3.5$. (c) Same as (a) for $\log_{10}T=4.2$.

$\log_{10}\rho$ (g/cm^3)	P (dyn/cm^2)	S (erg/g K)	U (erg/g)	c_v (Nk)
		(a)		
−6.0	2.0786×10^4	4.5877×10^8	−1.9026×10^{13}	1.500 00
−5.0	2.0787×10^5	4.1090×10^8	−1.9026×10^{13}	1.500 01
−4.0	2.0791×10^6	3.6304×10^8	−1.9026×10^{13}	1.500 07
−3.0	2.0838×10^7	3.1514×10^8	−1.9026×10^{13}	1.500 63
−2.0	2.1305×10^8	2.6693×10^8	−1.9026×10^{13}	1.506 38
−1.0	2.6337×10^9	2.1570×10^8	−1.9025×10^{13}	1.567 19
−0.5	1.4010×10^{10}	1.8355×10^8	−1.9019×10^{13}	1.739 73
+0.0	2.0146×10^{11}	1.3098×10^8	−1.8963×10^{13}	2.430 36
+0.5	5.2898×10^{12}	4.2822×10^7	−1.8240×10^{13}	3.569 97
		(b)		
−6.0	6.5732×10^4	4.9466×10^8	−1.8959×10^{13}	1.500 00
−5.0	6.5733×10^5	4.4680×10^8	−1.8959×10^{13}	1.500 00
−4.0	6.5744×10^6	3.9894×10^8	−1.8959×10^{13}	1.500 05
−3.0	6.5849×10^7	3.5105×10^8	−1.8959×10^{13}	1.500 49
−2.0	6.6895×10^8	3.0297×10^8	−1.8958×10^{13}	1.504 95
−1.0	7.7352×10^9	2.5300×10^8	−1.8955×10^{13}	1.549 86
−0.5	3.4419×10^{10}	2.2426×10^8	−1.8943×10^{13}	1.663 65
+0.0	3.0971×10^{11}	1.8483×10^8	−1.8863×10^{13}	2.075 59
+0.5	5.7465×10^{12}	1.2362×10^8	−1.8091×10^{13}	2.973 35
+1.0	9.0927×10^{13}	5.6801×10^7	−1.2949×10^{13}	4.507 10
		(c)		
−6.0	3.2944×10^5	5.4492×10^8	−1.8563×10^{13}	1.501 99
−5.0	3.2944×10^6	4.9706×10^8	−1.8563×10^{13}	1.501 94
−4.0	3.2947×10^7	4.4919×10^8	−1.8563×10^{13}	1.501 60
−3.0	3.2976×10^8	4.0132×10^8	−1.8563×10^{13}	1.501 09
−2.0	3.3259×10^9	3.5336×10^8	−1.8562×10^{13}	1.503 05
−1.0	3.5859×10^{10}	3.0457×10^8	−1.8549×10^{13}	1.529 21
−0.5	1.3446×10^{11}	2.7868×10^8	−1.8517×10^{13}	1.588 35
+0.0	7.3025×10^{11}	2.4889×10^8	−1.8369×10^{13}	1.773 85
+0.5	7.5470×10^{12}	2.1114×10^8	−1.7429×10^{13}	2.233 74
+1.0	9.7210×10^{13}	1.6449×10^8	−1.2122×10^{13}	2.946 32

TABLE III. Ground state occupation probability ω_1 as a function of the density for three isotherms.

$\log_{10}\rho$	ω_1 ($\log_{10}T = 3.0$)	ω_1 ($\log_{10}T = 3.5$)	ω_1 ($\log_{10}T = 4.2$)
-6.0	$1.0000 \times 10^{+0}$	$1.0000 \times 10^{+0}$	1.0000×10^{-0}
-5.0	9.9997×10^{-1}	9.9998×10^{-1}	9.9999×10^{-1}
-4.0	9.9974×10^{-1}	9.9981×10^{-1}	9.9990×10^{-1}
-3.0	9.9740×10^{-1}	9.9818×10^{-1}	9.9902×10^{-1}
-2.0	9.7438×10^{-1}	9.8209×10^{-1}	9.9035×10^{-1}
-1.0	7.7388×10^{-1}	8.3919×10^{-1}	9.1264×10^{-1}
-0.5	4.4614×10^{-1}	5.8248×10^{-1}	7.6170×10^{-1}
$+0.0$	8.4808×10^{-2}	1.9493×10^{-1}	4.4882×10^{-1}
$+0.5$	3.3414×10^{-3}	2.1425×10^{-2}	1.5278×10^{-1}
$+1.0$	2.4400×10^{-4}	2.8249×10^{-3}	5.0872×10^{-2}

A. Effect of the softness of the potential

In order to test the accuracy of the equation of state derived from the free-energy model (19), we have computed single- and double-shock Hugoniots, corresponding to the shock-wave experiments performed by Nellis and his collaborators [1]. These experiments probe the behavior of fluid He up to 20 000 K and 0.6 Mbar. Figure 2 shows the Hugoniot curves derived from our model, with the effective potential (2). The theoretical curve matches all the experimental data for the single and the double shock within the error bars. The initial conditions are the same as those of Nellis et al., i.e., the pressure

calculated from our free-energy model (19) at $T = 4$ K and $V = 32.4$ cm^3/mole. Pressure and internal energy for some representative points along the theoretical single-shock and double-shock Hugoniot curves are given in Table IV, parts (a) and (b), respectively.

Another test for the reliability of our model is the comparison with experimental results obtained for the speed of sound. Figure 3 shows the comparison between the experimental speed of sound $c_S = \sqrt{(\partial P/\partial \rho)_S}$ at $T = 298$ K [27] and the value derived from our free-energy model, with the potential (2), up to a density $\rho \approx 1$ g cm^{-3}, i.e., $P \approx 1.5 \times 10^{-1}$ Mbar. The agreement is excellent, even though the simple density dependence included in (2) is a
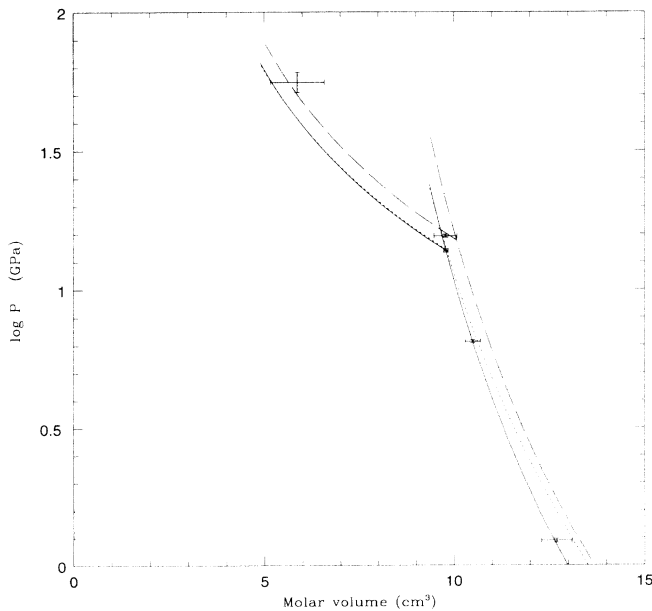

FIG. 2. Single- and double-shock Hugoniot curves for He. The experimental data are from Nellis et al. [3]. The solid curve is the theoretical curve obtained with the potential (2) and the related optimized parameters (see Secs. III A and V A) in our free-energy model (19). The dotted line is the theoretical curve obtained when using the potential of Nellis et al. in our calculations (see Sec. III A), whereas the long-dashed line is obtained with the Ceperley-Partridge potential [1].

TABLE IV. (a) Points along the helium single-shock Hugoniot curve, derived from the free energy model (19). The initial conditions are the experimental ones [3]: $V_{mol} = 32.4$ cm^3 and $P = 1$ atm. (b) Same as (a) for the double-shock, reflected from the experimental point $V_{mol} = 9.8$ cm^3.

| V_{mol} (cm^3/mol)	T (K)	P (GPa)	U (erg/g)
	(a)		
13.587	474.51	0.7127	-1.9039×10^{13}
12.764	762.63	1.1352	-1.9028×10^{13}
12.034	1258.4	1.8297	-1.9009×10^{13}
11.384	2111.6	2.9740	-1.8977×10^{13}
10.800	3587.2	4.8729	-1.8924×10^{13}
10.273	6175.5	8.0765	-1.8832×10^{13}
9.795	10852.	13.660	-1.8669×10^{13}
9.360	19788.	23.972	-1.8365×10^{13}
	(b)		
9.7874	10963	13.790	-1.8666×10^{13}
8.8976	11775	16.693	-1.8632×10^{13}
8.1561	12598	19.932	-1.8597×10^{13}
7.5287	13456	23.553	-1.8560×10^{13}
6.9910	14373	27.613	-1.8521×10^{13}
6.5249	15371	32.175	-1.8478×10^{13}
6.1171	16475	37.318	-1.8431×10^{13}
5.7573	17711	43.130	-1.8379×10^{13}
5.4374	19110	49.720	-1.8320×10^{13}
5.1512	20706	57.217	-1.8254×10^{13}
4.8937	22542	65.776	-1.8179×10^{13}
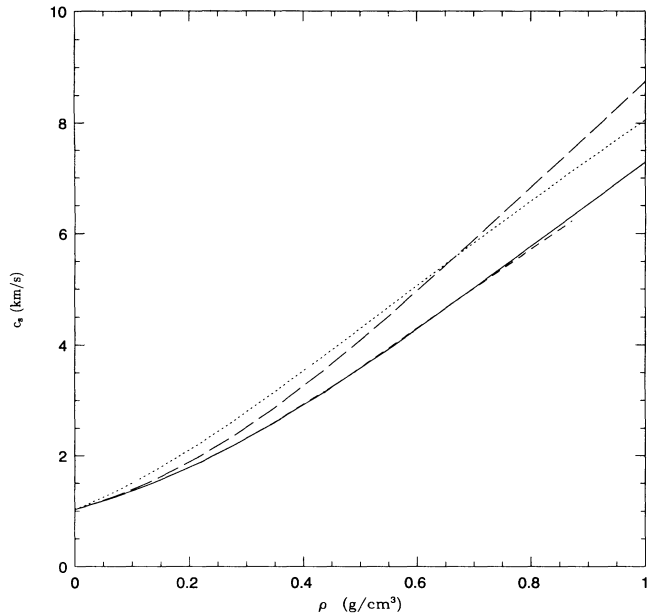
FIG. 3. Comparison between the experimental [27] (short-dashed line) and the theoretical (solid line) speed of sound at $T=298$ K as a function of the density. Also shown are the resulting curves when the potential of Nellis *et al.* (dotted) or the regular Ceperley-Partridge potential (long-dashed) is used in the calculations.

FIG. 4. Hard-sphere diameters σ_{WCA} of He (solid), and breakpoint λ_{BP} (dashed) along the following isotherms: $\log_{10}T=3$, $\log_{10}T=3.5$, $\log_{10}T=4$, and $\log_{10}T=4.5$, from top to bottom.

crude description of the many-body contribution to the interparticle potential. In view of these comparisons, we elected to choose the potential (2), with the optimized parameters given above, within all the range of temperature and density of interest.

We stress the fact that the comparison with the shock-wave experiments is, to some extent, probing only the *qualitative* behavior of the model, since the parameters in the potential are adjusted to reproduce the results. The speed of sound experiments, on the other hand, provide a stringent test for the *quantitative* behavior of the model, since *no* parameter is further adjusted in this case. Therefore, our model, with the *fixed* parameters C and D in the effective pair potential (2), reproduces both shock-wave and acoustic experiments within the whole temperature and density range presently available. These comparisons assess the validity of our model at high temperature and high density, at least in the domain currently covered by static and dynamic experiments.

The importance of the softening of the potential (i.e., its density dependence) clearly appears in Figs. 2 and 3. The *ab initio* Ceperley-Partridge potential provides an accurate low-density limit but fails to reproduce high-density data (the shock-wave experiments are never in the low-density regime). On the other hand, the Nellis *et al.* potential accurately reproduces the shock-wave experiments (by construction), but does not reproduce the speed of sound experiments (about 15% departure at high density). These calculations show convincingly the necessity to include a density dependence in the repulsive part of the potential, even as crudely as in Eq. (2), to reproduce both sets of experimental data.
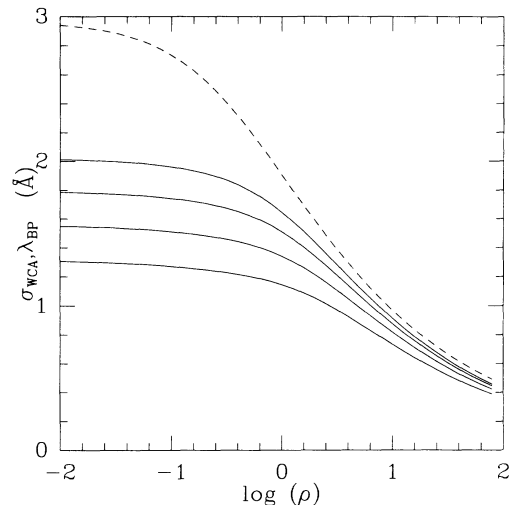
B. Density and temperature dependence of the hard-sphere radii

Figure 4 shows the density dependence of the hard-sphere diameters $\sigma_{WCA}(\rho,T)$, corresponding to the ground state of helium atoms, along a few isotherms. The diameters are found to be nearly constant for a given temperature up to a density $\rho\approx10^{-1}$ g cm^{-3}, decreasing with increasing temperature, and then to decrease rapidly with increasing density, converging eventually to the breakpoint value $\sigma=\lambda=a_{fcc}$ at high density. We stress that this strong dependence of the ground state diameter, and then of the configuration free energy, on the density is essential to give a reliable description of the thermodynamic properties of matter at high pressure, and in particular of the impending phenomenon of pressure ionization. Any theoretical model which relies on hard-sphere models for the interaction between neutral particles must include a *consistent density and temperature dependence* of the hard-sphere diameters.

C. Low-excitation and low-density approximations

Figure 5 shows the relative populations of the first six states, i.e., $n=1-3$ for all l, as given by Eqs. (10) and (17), for $T=10^5$ K. Substantial temperature ionization, which is not included in the present model, occurs at this temperature, but we just want to illustrate the density dependence of the internal states, within the present formalism. The behavior is qualitatively identical for lower temperatures, but the excited levels are less populated [$\log_{10}(N_{i>1}/N)\lesssim-10$ for $\log_{10}T\leq4.2$]. The general features can be explained as follows: At low density, the ratio N_i/N_1 is a direct measure of the degree of thermal excitation. As the density increases, Fig. 5 shows the strong density dependence of the IPF, and the state by
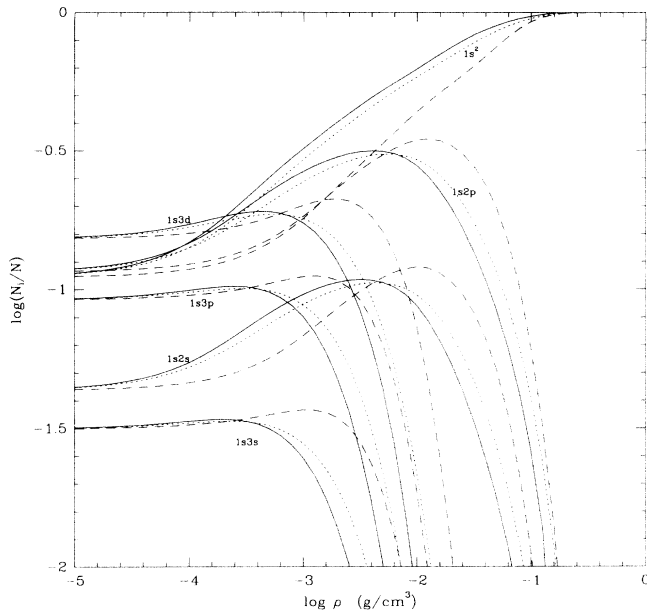
FIG. 5. Relative populations $\log_{10}(N_i/\sum_i N_i)$ for $n = 1$–3, for all l, as a function of density for $\log_{10}T = 5$. The solid line represents the complete calculation, beyond the low-density approximation and the low-excitation approximation, the dotted line shows the results of the calculations within the LDA, and the dashed line represent the results within the LDA and the LEA. Note that ten states were included in the present calculations ($n = 1 \rightarrow 4$), but only the first ones are shown.

state cutoff of each excited state. Highly excited states are removed first as the density increases, a direct consequence of the larger volume they occupy in the phase space [Eq. (14)] and the related decreasing occupation probability [Eqs. (15) and (17)]. Within the temperature range of interest in the present paper, however, helium atoms remain essentially in their ground state. This minimizes the error made by factorizing out the internal and configurational parts of the partition function in the treatment of N-body effects [Eq. (1)].

Figure 5 also shows the results obtained within the low-density approximation (but *no* low-excitation approximation) (dotted line), and within the low-density approximation *and* the low-excitation approximation (dashed line). As seen in the Figure, the low-density approximation [Eq. (15)] can be safely used even at high density. This is not true for the low-excitation approximation, at least for the highest temperatures, where thermal excitation becomes substantial. When terms beyond the LEA are included, *all* particles surrounding a given one can be in an excited state $n > 1$, hereby experiencing stronger interactions [see Eq. (15)] than within the LEA. Then, above a certain density, the population of the highly excited states will decrease, thereby increasing the population of the *lower* excited states, since $\sum_i N_i = N$ [see Eqs. (10), (14b), (15), and (17)]. At very high density, the ground state will be the ultimately populated state.

This shows the importance of going beyond the low-excitation approximation in the calculation of the internal levels population *at high density* as soon as substantial

thermal excitation, and the impending thermal *ionization*, takes place. Though of limited interest within the limits of the present model ($\log_{10}T < 4.2$), where thermal excitation remains negligible, this might be of prior importance at high pressure and temperature, when ionization will set in.

D. Importance of the self-ionizing states

For the sake of completeness, we have concluded some calculations including the $2s^2$ state in the IPF. As discussed earlier, the occupation probability of this state can become larger than the one of certain singly excited states, because of the larger volume occupied by the latter at high density. At any rate, the contribution of the doubly excited states is found to be always negligible in the density and temperature range of interest $[\log_{10}(N_{[2s^2]}/N) < -4$ at $T = 10^5$ K$]$.

E. Quantum effects

We have taken into account quantum, diffraction effects between particles, by using the well-known semi-classical $\hbar$-(Wigner-Kirkwood) expansion in the free energy [21]. Truncation of the expansion at the order $\hbar^2$ leads to the well-known term (19d). We stress the fact that the pair distribution function entering the perturbation term (19d) must be approximated by

$$g(r) \approx y_{HS}(r)e^{-\beta\phi(r)},$$

where $\phi(r)$ is the *true* potential, and not by $g(r) \approx g_{HS}(r)$. This difference is inconsequential when considering the pair distribution function (PDF) of the *reference* optimized hard-sphere potential, but no longer when the *true* potential is used, as in the Wigner-Kirkwood expansion. The second solution leads to an overestimation of $g(r)$ at short distances, and then to an overestimation of the quantum correction. This is of prior importance when calculating the initial conditions for the Hugoniots at 4 K, where quantum effects become substantial.

The $\hbar$ expansion is valid as long as quantum effects are weak and can be treated as a perturbation of the classical interaction. At high density *and* low temperature, this approximation breaks down, and leads to unphysical results, such as negative specific heat c_v. That puts a limit on the validity of our model. We used the criterion $c_v > 1$ in units of Nk as the validity condition for our model. This corresponds to $\log_{10}T - \log_{10}\rho \gtrsim 2$. Such a limitation has no consequences for astrophysical applications, since no helium-rich astrophysical objects lie in this temperature-density domain.

VI. RELATIVE IMPORTANCE OF THE DIFFERENT CONTRIBUTIONS TO THE FREE ENERGY

Figures 6(a)–6(d) show the relative importance of the different contributions to the free energy along represen-

tative isotherms. The vertical scale is the logarithm of the absolute value of the free energy in units of NkT. Positive and negative contributions are labeled (>0) and (<0), respectively. The various contributions are described in the caption. In order to separate out the contributions arising from the configuration term (ground state interactions) and from the internal structure (excited states interactions), we have rewritten Eqs. (19b) and (19c) as follows:

$$\frac{\beta F_{\text{int}}(\{N_i\}, V, T)}{N}$$
$$= -\ln \sum_i \omega_i g_i e^{-\beta \epsilon_i}$$
$$+ \beta \left[\frac{f_{\text{HS}}(\{N_i\}, V, T, \{\sigma_i\})}{N} - \frac{f_{\text{HS}}(N, V, T, \sigma_1)}{N} \right]$$
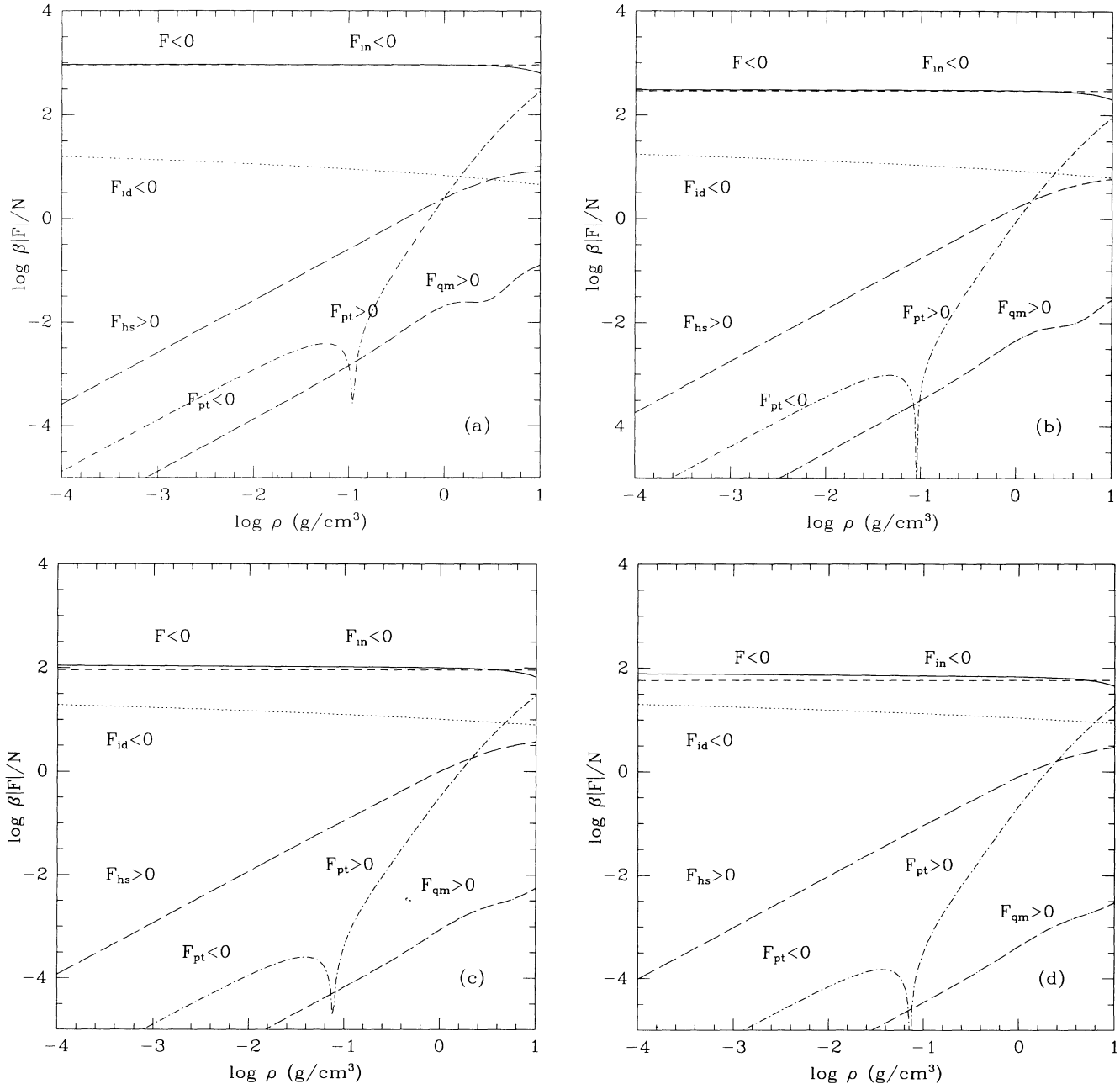$$- \sum_i N_i \beta \frac{\partial f_{\text{HS}}(\{N_i\}, V, T, \{\sigma_i\})}{\partial N_i} , \qquad (20a)$$

FIG. 6. Individual contributions to the Helmholtz free energy. The quantity plotted is $\log_{10}\beta|F|/N$. The total free energy is shown by the solid line. The different contributions, as defined respectively in Eqs. (19a), (19d), (20a), (20b) (the first term on the rhs), and (19c) are kinetic F_{id} (dotted line), quantum F_{qm} (long-dashed–dotted), internal F_{in} (short-dashed), reference F_{hs} (long-dashed), and perturbation F_{pt} (short dashed-dotted). (a)–(d) correspond, respectively, to $\log_{10}T=3$, $\log_{10}T=3.5$, $\log_{10}T=4$, and $\log_{10}T=4.2$.

$$\frac{\beta F_{\mathrm{conf}}(N,V,T)}{N} = \frac{\beta f_{\mathrm{HS}}(N,V,T,\sigma_1)}{N} + \frac{\beta F_{\mathrm{pert}}(N,V,T)}{N} ,$$

(20b)

where $f_{\mathrm{HS}}(N,V,T,\sigma_1)$ and $f_{\mathrm{HS}}(\{N_i\},V,T,\{\sigma_i\})$ denote, respectively, the free energy of a *one-component* and a *multicomponent* hard-sphere fluid, and F_{pert} is given by Eq. (19c).

As shown in the figure, the fluid is nearly ideal up to $\log_{10}\rho \sim -1$. The total free energy is essentially the sum

of the translational and the internal structure contributions for the isolated atom, whereas the configuration term remains negligible. As the density is raised, the positive, nonlinear combination of the hard-sphere energy in the configuration term increases, as well as the perturbation part, and becomes eventually of the order of the internal structure contribution. Note that, since the He-He potential (2) is negative at long distances (weak attraction) and positive at short distances (strong repulsion), the perturbation (HTA) term is negative at low density but positive at high density. Though small at low densi-
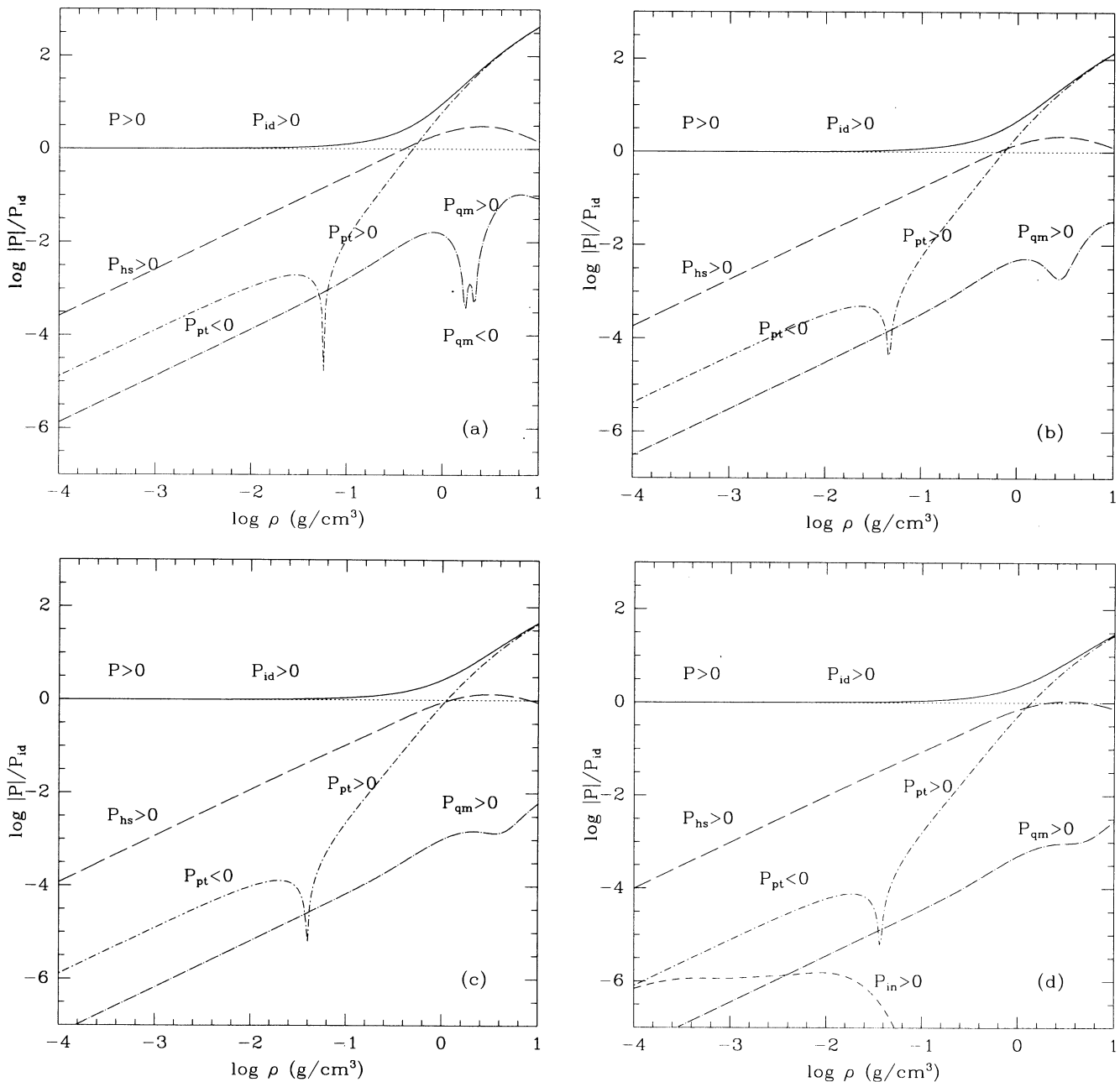

FIG. 7. Same as Figs. 6(a)–6(d) for the pressure. The legends are the same. The internal structure pressure is off scale for all but the $\log_{10}T = 4.2$ isotherms.

ty, this term becomes dominant at high density, a consequence of the density-dependent potential separation of Kang *et al.* which moves towards small r regions, i.e., stiffer parts of the potential, as the density increases. At this point, the fluid is highly nonideal, and eventually the total free energy is dominated by the configuration term. This behavior shows the essential role of the softness of the potential at high density, as already shown by the strong density dependence of the hard-sphere diameter in this region. Again, this stresses the need for a self-consistent density dependence of the interaction in any model aimed at describing the thermodynamics of fluids at high density and high temperature.

The effect of these strong, nonideal interactions is also felt in the internal structure contribution, as states are removed from the IPF. The occupation probabilities ω_α decrease with increasing density above $\log_{10}\rho \gtrsim -2$, thereby raising the internal energy [see Eqs. (7)–(9)]. Note that the ground state contribution ($i = 1$) enters the *configuration* term (20b), and not the internal structure term (20a), so that the strong density dependence of ω_1 (see Table III) is reflected in the configuration energy. The term $[f - \sum_i (\partial f/\partial N_i)]$, which is exactly zero in the low-density plus low-excitation approximation [19,5], remains small compared with the term $-NkT \ln \widetilde{Z}$. The behavior of the internal structure term becomes dubious above $\log_{10}\rho \gtrsim 1$, where pressure ionization is expected so that the ground state itself will be removed eventually in the continuum ($\omega_1 \rightarrow 0$). The quantum correction remains always small within the limit of validity of our model, as stated previously.

Each of the contributions to the free energy presented in Fig. 5 displays a similar, general density dependence for all the isotherms. The internal contribution shows almost no variation at low density, as long as $\omega_i \sim 1$ $\forall i$, and then increases slightly as $\omega_i \rightarrow 0$ at high density. Since the atoms remain in their ground state under the conditions examined here, this contribution is essentially the binding energy of the helium atom with respect to the He^{2+} ion. The configuration term depends strongly on the density. It is dominated by the hard-sphere term at low density. Above $\log_{10}\rho \gtrsim 0$, this term and the perturbation part strongly increase with the density and become eventually dominant, as discussed above. The quantum contribution increases strongly with density, as expected.

The temperature dependence does not affect this behavior from the qualitative viewpoint, but is reflected by the quantitative contribution of each term. The configuration term decreases at higher temperature as the gas becomes more ideal. The internal free energy is nearly independent of the temperature since, within the temperature range of interest, the atoms remain essentially in their ground state. The quantum contribution decreases monotonically with temperature since $F_{qm} \propto 1/T$ in a first approximation.

For the sake of completeness, we show the various contributions to the pressure in Figs. 7(a)–7(d) for the same isotherms. We recover the same qualitative and quantitative features. The contribution of the internal structure to the pressure is completely negligible, reflecting the near density independence of the internal free energy.

The total pressure is largely dominated by the configuration term in the nonideal regime at high density ($\log_{10}\rho \gtrsim -1$).

We can summarize the general behavior of the thermodynamics of dense atomic helium, as described by our model, as follows.

(i) The fluid is nearly ideal up to $\log_{10}\rho \sim -1$ ($P^{ex}/P^{tot} \approx 2.5\%$ and $S^{ex}/S^{tot} \approx 1.6\%$ for $\log_{10}\rho = -1$ and $\log_{10}T = 3$). The effect of strong correlations becomes important, and even dominant, at higher densities.

(ii) The atoms remain essentially in their ground state in the temperature range considered in the present paper, i.e., $\log_{10}T \leq 4.2$.

(iii) The correlation term is essentially dominated by the hard-sphere term, linear in density in a first approximation, up to $\log_{10}\rho \lesssim -1$. Then nonlinear terms, both in the reference and in the perturbation parts, become important and the correlation term eventually dominates at high density. It decreases slowly with T.

(iv) The internal structure contribution, the major contribution to the total free energy besides the pure translational term at low density, is essentially the binding energy of the helium atom, a consequence of point (ii), and then is nearly constant within the density and temperature range of interest. Consequently, its contribution to the pressure is negligible.

(v) The quantum contribution is the smallest at all densities and temperatures. This term, however, exhibits a very strong density dependence, leading to a non-negligible contribution to the pressure, and a dominant contribution to the specific heat, at high densities and low temperatures.

VII. CONCLUSION

We have developed a free-energy model for fluid atomic helium, which is intended to give a correct equation of state at high density and high temperature. The configuration energy is calculated within the framework of a perturbation theory, based on a realistic, effective *density-dependent* potential which includes N-body effects at high density and recovers the accurate Ceperley-Partridge potential at low density. This configuration energy is density and temperature dependent, through the thermodynamically determined hard-sphere diameters entering the reference free energy. The influence of the interactions on the internal levels of He is calculated *self-consistently* with an occupation probability. A scaling law between the internal atomic states has been developed, which relates the radius of the excited states to the radius of the ground state entering the configuration energy. This scaling law reproduces the energy spectrum of He within less than 3%, and the radius of the $1s^2$ wave function within less than 4%. We stress the importance of such a self-consistency between the configuration energy and the internal structure energy, and of the density dependence of the configuration energy, for a correct description of the fluid at high density. We extended previous calculations of the internal structure contribution beyond the so-called low-density and low-excitation approximations. Even though these two

approximations are found to be always valid within the limits of the present model, the low-excitation approximation leads to appreciable errors in the calculation of the level populations as soon as thermal excitation becomes substantial. This will be important when pressure ionization will be considered, since at high density, thermally excited *atoms* can survive in the midst of ions and free electrons.

This free-energy model reproduces accurately the available shock-wave experimental results and speed of sound measurements at high density. This assesses its validity in the high-density regime, where it provides a solid ground for a correct description of the properties of *dense* atomic helium at high temperature. It has immediate applications to the study of the outer layers of giant planets, brown dwarfs, and white dwarfs, and in the analysis of future shock-compression experiments. In a forthcoming paper, this model will be extended to the partially and fully ionized regions, in order to describe temperature and pressure ionization.

ACKNOWLEDGMENTS

[1] W. J. Nellis, N. C. Holmes, A. C. Mitchell, R. J. Train, G. K. Governo, M. Ross, and D. A. Young, Phys. Rev. Lett. **53**, 1248 (1984).

[2] G. Chabrier, D. Saumon, W. B. Hubbard, and J. I. Lunine, Astrophys. J. **391**, 817 (1992).

[3] I. Mazzitelli, in *The Equation of State in Astrophysics*, IAU Colloquium No. 147, edited by G. Chabrier and E. Schatzman (Cambridge University Press, Cambridge, England, 1994).

[4] G. Fontaine, in *The Equation of State in Astrophysics*, IAU Colloquium No. 147 (Ref. 3).

[5] D. Saumon and G. Chabrier, Phys. Rev. A **44**, 5122 (1991).

[6] D. Saumon and G. Chabrier, Phys. Rev. A **46**, 2084 (1992).

[7] R. A. Aziz, F. R. McCourt, and C. C. K. Wong, Mol. Phys. **61**, 1487 (1987).

[8] M. Ross, F. H. Ree, and D. A. Young, J. Chem. Phys. **79**, 1487 (1983).

[9] R. J. Hemley, H. K. Mao, L. W. Finger, A. P. Jephcoat, R. M. Hazen, and C. S. Zha, Phys. Rev. B **42**, 6458 (1990).

[10] D. M. Ceperley and H. Partridge, J. Chem. Phys. **84**, 820 (1986).

[11] J. D. Weeks, D. Chandler, and H. C. Andersen, J. Chem. Phys. **54**, 5237 (1971).

[12] H. S. Kang, C. S. Lee, T. Ree, and F. Ree, J. Chem. Phys. **82**, 414 (1985).

[13] D. Saumon, G. Chabrier, and J. J. Weis, J. Chem. Phys. **90**, 7395 (1989).

[14] G. A. Mansoori, N. F. Carnahan, K. E. Starling, and T. W. Leland, J. Chem. Phys. **54**, 1523 (1971).

[15] L. Verlet and J. J. Weis, Phys. Rev. A **5**, 939 (1972).

[16] E. W. Gründke and D. Henderson, Mol. Phys. **24**, 269 (1972).

[17] J.-P. Hansen and I. R. McDonald, *Theory of Simple Liquids* (Academic, New York, 1976), Sec. 6.6.

[18] J. D. Weeks, D. Chandler, and H. C. Andersen, J. Chem. Phys. **55**, 5422 (1971).

[19] D. G. Hummer and D. Mihalas, Astrophys. J. **331**, 794 (1988).

[20] W. C. Martin, J. Chem. Phys. Ref. Data **2**, 257 (1973).

[21] L. D. Landau and E. M. Lifschitz, *Statistical Physics* (Pergamon, New York, 1988), Sec. 33.

[22] R. V. Jensen, Nature **335**, 591 (1992).

[23] G. S. Ezra, K. Richter, G. Tanner, and D. Wingten, J. Phys. B **24**, L413 (1991).

[24] H. Bethe and E. E. Salpeter, in *Atoms*, edited by S. Flügge, Handbuch der Physik Vol. 35 (Springer-Verlag, Berlin, 1957), p. 231.

[25] K. Gottfried, *Quantum Mechanics* (Addison-Wesley, Reading, MA, 1989).

[26] C. L. Pekeris, Phys. Rev. **115**, 1216 (1959).

[27] R. LeToullec, P. Loubeyre, and J.-P. Pinceaux, Phys. Rev. B **40**, 2368 (1989).